Eur. Phys. J. Special Topics **160**, 165–174 (2008)

DOI: 10.1140/epjst/e2008-00720-1

THE EUROPEAN PHYSICAL JOURNAL SPECIAL TOPICS

Noise fluctuations and the Berry phase: Towards an experimental test

S. Filipp[a]

Atominstitut der Österreichischen Universitäten, Stadionallee 2, 1020 Wien, Austria

Abstract. Due to its geometric nature Berry's geometric phase exhibits stability to a great extent when exposed to parametric noise fluctuations. Considering an adiabatic evolution of a non-degenerate quantum system the variance of the geometric phase resulting from fluctuations vanishes as the evolution time tends to infinity. Here we present numerical data marking the domain of validity of the adiabatic approximation. We notice that due to second-order effects the variance does not vanish, but rather increases again for evolutions longer than a certain critical time. Furthermore, the occurence of a shift of the mean geometric phase is demonstrated and we give a simple geometrical description in terms of probability distributions of this effect. Finally, an experiment utilizing ultra-cold neutrons is proposed to verify the remarkable dephasing survival of the geometric phase.

1 Introduction

The first reference to a geometric phase in quantum mechanics dates already back to the work of Pancharatnam in 1956 [1]. However, it was Berry who manifested the notion of the quantum geometric phase accompanying the cyclic and adiabatic transport of a quantum state [2]. His seminal paper lead to numerous further investigations in various directions [3], e.g. to non-adiabatic [4], non-cyclic and non-unitary evolutions [5], degenerate subspaces [6], or mixed states [7]. Especially the potential advantages of quantum geometric gates for quantum information processing has been topic of recent investigation [8–10] since its geometric origin provides protection against certain classes of noise influences [11,12].

The concept of the Berry phase can be illustrated most easily by means of a spin-1/2 particle in a magnetic field, for example a neutron. This is also the reason of an abundance of experiments on Berry's geometric phase using neutrons [13]. In brief, the spin of the neutron follows adiabatic variations of a magnetic field. If the spin is initially aligned with the magnetic field and the field direction traces out a closed loop, the final and initial state will be equivalent up to a phase factor. Simply solving the time-dependent Schrödinger equation and neglecting non-adiabatic terms leads to two complementary contributions to the final phase factor, a *geometric* part ϕ_g and a *dynamical* part ϕ_d. The latter depends on the evolution time and the Zeeman energy, whereas the former depends only on the path traced out by the magnetic field vector: It is proportional to the surface area of the path enclosed by the state in state space. Put into equations, these phases are given by

$$\phi_g = \int_{R(0)}^{R(T)} \langle n(\boldsymbol{R}(t))|\nabla_{\boldsymbol{R}}|n(\boldsymbol{R}(t))\rangle d\boldsymbol{R} \qquad \text{and} \qquad \phi_d = \int_0^T E_n(t)/\hbar\, dt, \tag{1}$$

where the parameters $\boldsymbol{R}(t)$ denote the change of the Hamilton-operator $H(\boldsymbol{R}(t))$ in the time interval $t \in [0, T]$. T denotes the period of the cyclic evolution. Its eigenstates $|n(t)\rangle$ change

[a] e-mail: sfilipp@ati.ac.at

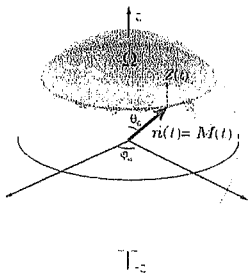

Fig. 1. Bloch-sphere picture of the spin-1/2 state evolving adiabatically in a (fluctuating) magnetic field. The vector denotes the polarization vector of the spin state $\boldsymbol{M}$ as well as the direction of the magnetic field $\boldsymbol{n}$.

accordingly and the instantaneous energy is given by $E(t) = \langle n(t)|H(t)|n(t)\rangle$ (skipping the dependency on the parameters $\boldsymbol{R}$ for notational convenience).

In the particular case of neutrons the Hamiltonian

$$H(t) = -\mu_n \boldsymbol{\sigma} \cdot \boldsymbol{B}(t) \tag{2}$$

describes the coupling of the neutrons' spin angular momentum to the magnetic field $\boldsymbol{B}(t) = B(t)\boldsymbol{n}(t)$ with magnitude $B(t) \equiv |\boldsymbol{B}(t)|$ and direction determined by the unit vector $\boldsymbol{n}(t) = (\sin\theta_0(t)\cos\varphi_0(t), \sin\theta_0(t)\sin\varphi_0(t), \cos\theta_0(t))^T$. $\boldsymbol{\sigma} = \{\sigma_x, \sigma_y, \sigma_z\}$ denote the Pauli matrices and $\mu_n = -9.66 \times 10^{-27}$ J/T the magnetic moment of the neutron. The instantaneous spin state $|\psi(t)\rangle = \cos(\theta(t)/2)|z+\rangle + e^{i\varphi(t)}\sin(\theta(t)/2)|z-\rangle$ can be depicted on the Bloch-sphere in the fixed basis $\{|z+\rangle, |z-\rangle\}$ which are the eigenstates to the σ_z operator, $\sigma_z|z\pm\rangle = \pm|z\pm\rangle$. The direction of the magnetic field and the polarization vector $\boldsymbol{M} = \langle\psi|\boldsymbol{\sigma}|\psi\rangle$ coincide at all times for an adiabatic transport. ϕ_g can then be expressed in terms of the solid angle Ω enclosed by the path on the Bloch sphere, $\phi_g = -\Omega/2$, stressing therewith its independence of energy and time. For a path tracing out a conic section with constant polar angle θ_0 and $\varphi \in [0, 2\pi]$ (c.f. solid red curve in Figure 1) the geometric phase is given by

$$\phi_g = -\pi(1 - \cos\theta_0), \tag{3}$$

whereas the dynamical phase is given by the integral $\phi_d = \mu_n/\hbar \int_0^T B(t)dt$.

2 Stability of the geometric phase

Fluctuations in the magnetic field will affect both phases, and the question is whether they show different characteristics. The statistical spreads of the geometric and the dynamical phase when averaging over several paths turns out to depend on the total evolution time T in a different way. Whereas for the variance of the dynamical phase a usual diffusive behaviour is expected, i.e. a linear increase of the variance with increasing T, calculations in first-order perturbation theory show that the variance of the geometric phase under the influence of adiabatic noise is proportional to the inverse time and eventually vanishes as the change rate of the Hamiltonian tends to zero [14]. It is illustrative to explicate this feature with a geometrical picture in mind. Fluctuations in the path lead to changes in energy and therefore the integral of these energy changes in the time domain leads to diffusion, just like a particle diffuses in a Brownian motion process. In contrast, the geometric phase is neither determined by energy changes nor by the evolution time, but only by the area enclosed by the path on the Bloch-sphere. Extending the evolution time translates into an increase of the relative frequency of the fluctuations with respect to the constant path length. The wiggles have enough time to average out and the area enclosed by the fluctuating path increasingly equals the unperturbed area in each noise realization.

In detail, the modified Hamiltonian when adding (adiabatic) fluctuations is given by

$$H(t) = -\mu_n \boldsymbol{B}(t) \cdot \boldsymbol{\sigma} - \mu_n Z(t)\sigma_z. \tag{4}$$

The first term denotes the unperturbed evolution according to Eq. (2) and the second term the noise fluctuations. Since – according to De Chiara and Palma [14] – there is no essential difference in the behaviour of the variance of the geometric phase, instead of an isotropic noise distribution we take the noise fluctuations pointing in z-direction, i.e. along the axis of the cone formed by the path on the Bloch sphere. Assuming an Ornstein-Uhlenbeck noise process (Gaussian, stationary and Markovian [16]) the variance of the geometric phase $\sigma^2_{\phi_g}$ can be derived analytically in first-order perturbation theory [14] and is given by

$$\sigma^2_{\phi_g} = 2P^2 \left(\frac{\pi \sin^2 \theta_0}{T\omega_L} \right)^2 \left[\frac{\Gamma_n T - 1 + e^{-\Gamma_n T}}{\Gamma_n^2} \right]. \tag{5}$$

$P = \mathrm{var}(Z)$ denotes the variance of the Gaussian distributed random variable Z and, therefore, the strength of the noise. $\omega_L = 2\mu|B|/\hbar$ stands for the Larmor frequency determined by the Zeeman energy splitting in the magnetic field of strength $|B|$, and Γ_n for the bandwidth (HWHM) of the Lorentzian noise power spectrum.

The following assumptions have been made: First, $\Gamma_n \ll \omega_L$ and $\omega_r \equiv 2\pi/T \ll \omega_L$ such that neither the noise frequency bandwidth nor the angular velocity of the evolution ω_r exceeds the Larmor frequencies in order to guarantee adiabaticity throughout the evolution time. Second, the perturbations must be small compared to the magnitude of the magnetic field, $P \ll \omega_L$, or, in other words, the signal-to-noise ratio ω_L/P must be much larger than one. There are no restrictions on the relative values of Γ_n and ω_r. However, we want the variance to vanish which is the case for $T \gg 1/\Gamma_n$, i.e. for a wiggly path instead of a merely quasi-static offset of the initial magnetic field:

$$\sigma^2_{\phi_g} \overset{T \gg \Gamma_n^{-1}}{\longrightarrow} 2P^2 \left(\frac{\pi \sin^2 \theta_0}{\omega_L} \right)^2 \frac{1}{\Gamma_n T}. \tag{6}$$

We recognize that $\sigma^2_{\phi_g}$ tends to zero for $(\Gamma_n T)^{-1} \to 0$, i.e. if T is large enough.

In the following, Eq. (6) is numerically validated showing two particular effects that are not included in this first-order theory. On one hand we encounter a shift of the mean geometric phase depending on the polar angle θ_0 as well as on the noise strength. This shift does not arise from non-adiabatic terms, but arises also for perfectly adiabatic following: it can be explained purely by geometric reasoning as discussed below (section 5). On the other hand we notice the emergence of a finite time interval for the observation of the geometric phase, that is, the variance does not vanish but increases again after a certain time.

3 Numerical simulation

From Eq. (5) we notice that the variance scales with the inverse signal-to-noise ratio squared and due to the adiabaticity condition this quantity is much smaller than one. This in turn means that the contributions to the dephasing of the geometric phase are rather small either and it seems difficult to design an experimental test for the geometric dephasing. The parameters have to be chosen carefully close to the borderline to non-adiabaticity, therefore, numerical simulations are needed for the implementation of a prospective experiment. These consists of two parts: the evolution of the spin state has to be simulated by computing the time-dependent Schrödinger equation for the Hamiltonian in Eq. (4) numerically. Additionally, artificial noise with specific strength and controllable spectrum has to be generated.

3.1 Evolution algorithm for the spin state

Generally speaking, the task is to solve the time-dependent Schrödinger equation

$$i\frac{\partial}{\partial t}\psi(\boldsymbol{x}, t) = H\psi(\boldsymbol{x}, t), \tag{7}$$

where $\psi(\boldsymbol{x},t) \in \mathcal{H}_x \otimes \mathcal{H}_s$ is a tensor product state with a spatial part represented in $\mathcal{H}_x$ and a spin angular momentum part element of $\mathcal{H}_s$. With regard to the intended experimental setup (section 6) we can safely neglect the spatial dependency due to the differences in the energy scales of up to a factor 10^5 between the Zeeman energy of the spin levels (for magnetic fields in the Gauss-region) and kinetic energy terms. Moreover, we also assume a sufficiently homogeneous magnetic field such that only the time-dependence of the field is of importance. In this case, $\psi_t \equiv \psi(t)$ is a two dimensional normalized complex vector representing the spin state of the neutron and the solution of Eq. (7) is simplified considerably.

As the fluctuations are sufficiently slow we do not have to solve a stochastic differential equation, but the entire evolution will be treated fully deterministic for each realisation and the stochastic nature enters when averaging over several noise realisations. Formally solving Eq. (7) yields $\psi_{\Delta t} = exp(-\mathrm{i}H\Delta t/\hbar)\psi_0$ where we assume that the Hamiltonian is approximately time-independent during the small time intervall Δt. The Cayley form of the exponential operator $e^{-\mathrm{i}H\Delta t/\hbar}$ can be utilized to solve the Schrödinger equation by the Crank-Nicholson scheme. In detail, the Cayley transform V of an Hermitian operator A is defined by [18] $A = \mathrm{i}(1+V)(1-V)^{-1}$ with unitary V allowing for a norm-preserving finite difference equation. Explicitly, the exponential operator can be written as $e^{-\mathrm{i}H\Delta t/\hbar} \approx (1-\mathrm{i}H\Delta t/2\hbar)(1+\mathrm{i}H\Delta t/2\hbar)^{-1}$. This approximation is accurate to second-order in time and leads to an evolution of the form

$$\left(1+\frac{\mathrm{i}}{2\hbar}H\Delta t\right)\psi(t_{n+1}) = \left(1-\frac{\mathrm{i}}{2\hbar}H\Delta t\right)\psi(t_n). \tag{8}$$

The Hamilton operator taken from Eq. (4) is evaluated at the intermediate time $t_n + \Delta t/2$ with $t_n = n\Delta t$. According to the total evolution time T the state vector is iterated $N = T/\Delta t$ times with Δt chosen to be much smaller than the period of the Larmor frequency $\Delta t \ll 2\pi/\omega_L$. If all the adiabatic constraints are satisfied by the specific choice of the parameters, the polarisation of the final state should be equal to the polarisation of the initial state, but with different relative phase. Calculating the phase difference $\arg(\psi_0^\dagger\psi_T)$ and subtracting the accumulated dynamical phase $\phi_d = 1/\hbar\sum_j^N \arg(\psi_{t_j}^\dagger\psi_{t_j})\Delta t$ yields the geometric phase.

3.2 Construction of the noise

As for the numerical simulation of the noise fluctuations we resort to a Fourier series representation to model an Ornstein-Uhlenbeck (O.-U.) stochastic noise process. Its power spectrum is given by a Lorentzian curve with bandwidth $\Gamma_n = 1/\tau_n$ proportional to the inverse of the relaxation time τ_n. One method to obtain the wanted stochastic process is to decompose it into a Fourier sum of trigonometric functions with random amplitudes and/or phases [19]. We resort to the latter option and write down a sum of cosine functions with random phases ϕ_k uniformly distributed in the interval $[0, 2\pi]$ and fixed amplitude C_k,

$$X(t) = \sum_k C_k \cos(\omega_k t - \phi_k). \tag{9}$$

The amplitudes are determined by $C_k = \sqrt{S(\omega_k)\Delta\omega/\pi}$, where $S(\omega)$ is the power spectral density of the noise and $\Delta\omega \equiv (\omega_{k+1} - \omega_k)$ denotes the constant angular frequency increment. The O.-U. process is eventually obtained by inserting a Lorentzian distributed power spectral density,

$$S(\omega) = 4P^2\frac{\tau_n}{1+(\tau_n\omega)^2}. \tag{10}$$

The integral $\int S(\omega)d\omega/2\pi$ over all positive ω gives the intensity of the noise P^2 as a measure of the strength of the fluctuations. As for the technical details, the sum in Eq. (9) has to be terminated at some point where all significantly contributing frequencies are included and we have decided on seven times the noise bandwidth for the maximum frequency, $\omega_{max} = 7\Gamma_n$. The division of the frequency band into N_f parts of width $\Delta\omega$ is chosen such that the phase

difference at the final time T of two adjacent partial waves is much smaller (a factor four turns out to be sufficient) than 2π,

$$\Delta\omega T \ll 2\pi \quad \rightarrow \quad N_f = \omega_{max}/\Delta\omega \gg \frac{\omega_{max}T}{2\pi}. \tag{11}$$

3.3 Noise envelope function

To meet the condition of cyclicality we multiply the generated noise sequence by an envelope function $e(t)$ which vanishes for $t = 0$ and $t = T$ while showing a smooth transition to and from unity in between. One might argue that terms due to the non-cyclicality lead only to correction in second-order and should therefore be negligible. However, with regard to an experimental "proof-of-principle" test a spin-echo type measurement has to be used and therefore we have to assure that the final state is equivalent to the initial state up to a phase necessitating the application of an envelope function. The particular function used in our simulations has the form of a Fermi-step functions and a second inverted one in sequence yielding finally a smoothened rectangular pulse of width T:

$$e(t) = \left(1 + e^{-c(t-d)}\right)^{-1} - \left(1 + e^{-c(t-(T-d))}\right)^{-1}. \tag{12}$$

The parameters c and d define the smoothness of the edges (corresponding to the temperature) and the position of the step (Fermi-energy), respectively, which have to be chosen such that the perturbations are switched on and off adiabatically.

4 Standard deviation of the geometric phase

Using the algorithms described above the mean and the standard deviation of the geometric phase has been evaluated for different parameter sets. The particular values of the parameters are selected also with respect to their relevance for a neutron experiment with the Larmor frequency ω_L of the order of 1800–18000 rad/s (0.1–1 Gauss) and evolution times between milliseconds and seconds. In Figure 2 the resulting data (dots) along with the theoretically predictions (solid line) for the standard deviation of the geometric phase is shown. The computed mean geometric phase $\bar{\phi}_g$ is drawn on top, where the shaded region underneath indicates the exact unperturbed geometric phase $\phi_g^0 = 2.65$ rad which corresponds to an an opening angle of $\theta_0 = 9\pi/20$ rad. The thickness of the bar refers to a region of ± 0.1 rad about the mean. In each figure the standard error is calculated for $n = 80$ noise realizations at each time step and the error of the error is estimated via $\sigma_\sigma = \sigma_{\phi_g}/\sqrt{2n}$ assuming Gaussian distributed values. Both for σ_{ϕ_g} and the mean value $\bar{\phi}_g$ there is a very good agreement between the numerical data and theory (Figure 2(a)).

Note, however, that the standard deviation of the geometric phase is quite small for the weak noise scenario and the question is whether we can measure such weak contributions to the dephasing. This fact is an obstacle for an experimental verification, but on the other side this means that the geometric phase is stabilizing very quickly if the adiabaticity conditions are fulfilled so that the geometric phase might indeed be a good candidate for error resilient quantum state manipulations. In particular, when performing an interferometric measurement of the geometric phase intensity oscillations $I \propto 1 + \cos(\phi_g)$ are observed and from averaging over the Gaussian distributed phases of several noise realizations a damping of the amplitude by the factor $\nu = exp(-\sigma^2_{\phi_g}/2)$ follows , $I \propto 1 + \nu\cos(\bar{\phi}_g)$. To resolve this decrease in amplitude by experiment a variance $\sigma^2_{\phi_g}$ close to one is preferable and therefore the signal-to-noise ratio must not be too small.

In Figure 2(b) the Larmor frequency as well as the noise bandwidth is reduced and the intensity of the noise is enlarged in order to obtain a larger σ_{ϕ_g} which can eventually be tested by experiment. There is still a good agreement with theory and the Larmor frequency can be reduced even more (Figure 2(c)). Now we notice that the standard deviations drop from the time where the velocity of the evolution becomes faster than the Larmor frequency. In

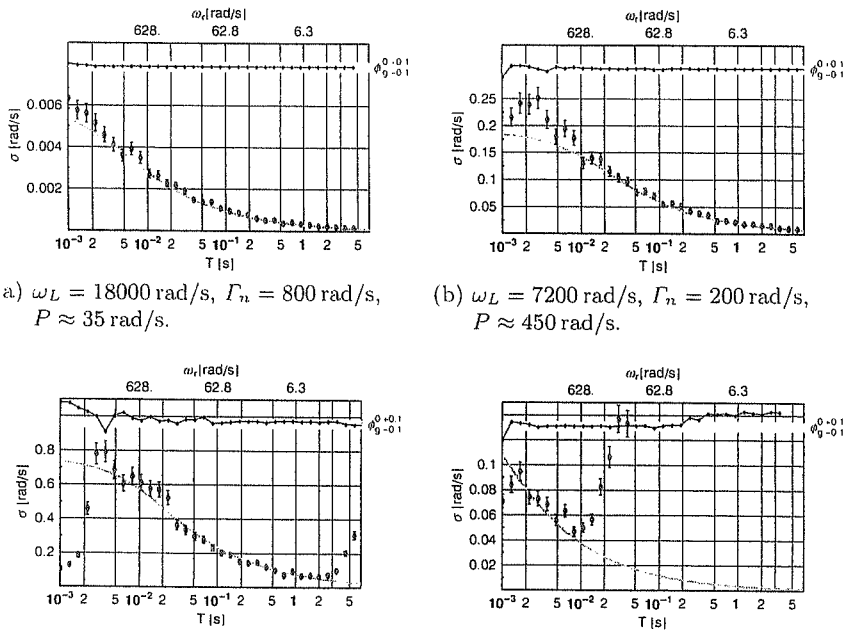

(a) $\omega_L = 18000\,\mathrm{rad/s}$, $\Gamma_n = 800\,\mathrm{rad/s}$, $P \approx 35\,\mathrm{rad/s}$.

(b) $\omega_L = 7200\,\mathrm{rad/s}$, $\Gamma_n = 200\,\mathrm{rad/s}$, $P \approx 450\,\mathrm{rad/s}$.

(c) $\omega_L = 1800\,\mathrm{rad/s}$, $\Gamma_n = 200\,\mathrm{rad/s}$, $P \approx 450\,\mathrm{rad/s}$.

(d) $\omega_L = 7200\,\mathrm{rad/s}$, $\Gamma_n = 5000\,\mathrm{rad/s}$, $P \approx 450\,\mathrm{rad/s}$.

Fig. 2. Standard deviation of the Berry phase for noisy paths plotted vs. the cyclic evolution time T with different parameters of the Larmor frequency $\omega_L = 2\mu_n B/\hbar$, the noise bandwidth Γ_n, and the noise strength P. On the top axis the angular velocity $\omega_r = 2\pi/T$ is given. The solid line indicates the theoretical curve from Eq. (5). On top the computed mean geometric phase is plotted shaded by the exact geometric phase $\phi_g = \pi(1 - \cos 9\pi/20) = 2.65\,\mathrm{rad}$, where the thickness indicates deviations $\pm 0.1\,\mathrm{rad}$.

this region also the mean geometric phase differs considerably from its unperturbed value and it becomes also apparent that for a smaller energy splitting the theory breaks down for long evolution times as well: a minimum of σ_{ϕ_g} is found at a critical evolution time. This effect has already been pointed out in [12,15], namely that there is a finite time-scale for a measurement of the geometric phase which can be attributed to the broadening of the systems energy levels due to the coupling to an environment. This minimum depends on the signal-to-noise ratio and on the noise spectrum – increasing the bandwidth of the noise leads to an even shorter time interval where the adiabatic approximation is valid – c.f. Figure 2(d).

5 Shift of the mean geometric phase

In the numerical data a difference between the unperturbed geometric phase $\phi_g^0 = -\pi(1 - \cos\theta_0)$ and the mean geometric phase $\bar{\phi}_g = -\pi(1 - \cos\bar{\theta})$ has been detected (Figure 3(b)) which depends on the intensity of the noise and the opening angle of the path. This result is not included in the first-order theory discussed above. Our aim is now to point out the very intuitive nature and geometric origin of this shift complementing the thorough calculations of the Berry phase in a non-isolated system coupled to a bath of harmonical oscillators by Whitney and Gefen [15].

The random variable Z in the Hamiltonian in Eq. (4) has a Gaussian symmetric probability distribution and therefore in the average we expect no contribution to the mean geometric phase. However, since the geometric phase game plays on a manifold with intrinsic curvature, a sphere, there arise non-linear terms in Z. The map of the stochastic process onto a sphere leads to an asymmetric probability distribution function that gives eventually rise to a shift of the geometric phase.

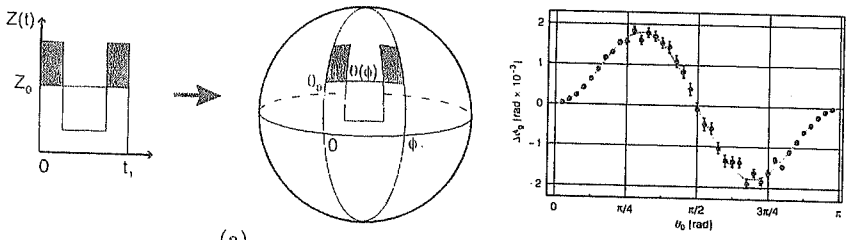

(a) (b)

Fig. 3. Fluctuating z-component of the magnetic field is mapped onto the spherical state space (a) leading to a shift of the mean geometric phase (b). The data points indicate the difference $\Delta\phi_g$ between unperturbed geometric phase and its mean value averaged over 400 noise realizations for each polar angle θ_0. The solid line shows the fit to the theoretical value determined by Eq. (18).

In Figure 3(a) a function $Z(t)$ is indicated that fluctuates about some mean value Z_0 such that the area above and below Z_0 are equal. Mapping this function onto a sphere such that the former mean Z_0 is mapped to θ_0 we notice that the weights above and below θ_0 are not equal anymore due to the curvature of the sphere. The new mean value $\bar{\theta}$ will therefore be different from θ_0 depending on the particular value of θ_0. In the limit where $\theta_0 = 0$ or π, i.e. at the north or south pole, there is no enclosed area anymore and therefore no difference between θ_0 and $\bar{\theta}$. For $\theta_0 = \pi/2$, at the equator, we do not expect any difference either due to the symmetry of the weights above and below the equatorial line. However, for all other values of θ_0 a slight change of the mean polar angle and therefore of the mean geometric phase is anticipated.

In detail, assuming that the fluctuations in the z-component are Gaussian distributed with mean $z_0 = B_z$ and variance s^2 the probability distribution function of the random variable Z is given by

$$p_Z(z) = \frac{1}{\sqrt{2\pi s^2}} e^{-(z-z_0)^2/2s^2}. \tag{13}$$

On the other hand the corresponding polar angle is given by

$$\tan\theta = \frac{B_r}{Z}, \qquad B_r = (B_x^2 + B_y^2)^{1/2} \tag{14}$$

and its probability distribution function p_Θ follows from the substitution rule of calculus,

$$p_\Theta(\theta) = p_Z(f^{-1}(\theta)) \left| \frac{df^{-1}(\theta)}{d\theta} \right| = \frac{B_r}{\sin^2\theta} p_Z\left(\frac{B_r}{\tan\theta}\right), \tag{15}$$

where f denotes the map

$$f : \begin{cases} Z \in (-\infty, 0) \mapsto \vartheta = \pi + \arctan\frac{B_r}{Z} \in (\pi, \pi/2) \\ Z \in (0, \infty) \mapsto \vartheta = \arctan\frac{B_r}{Z} \in (\pi/2, 0). \end{cases} \tag{16}$$

Inserting Eq. (13) into Eq. (15) finally yields

$$p_\Theta(\theta) = \frac{r}{\sqrt{2\pi}\sin^2\theta} \exp\left[-\frac{r^2}{2}\left(\frac{1}{\tan\theta} - \frac{1}{\tan\theta_0}\right)^2 \right] \tag{17}$$

with the ratio $r = B_r/s$ of the magnitude of the magnetic field perpendicular to the noise direction to the variance of the noise. Finally, the first moment of this distribution provides the mean polar angle

$$\bar{\theta} = \int \theta\, p_\Theta(\theta) d\theta \tag{18}$$

for calculating the mean geometric phase $\bar{\phi}_g = -\pi(1 - \cos\bar{\theta})$.

In Figure 3(b) the difference $\Delta\phi_g \equiv \bar{\phi}_g - \phi_g^0$ between the computed mean geometric phase $\bar{\phi}_g$ and the unperturbed geometric phase ϕ_g^0 is plotted for different cone opening angles θ_0. The parameter values $\omega_L = 3600\,\mathrm{rad/s}$, $P = 112\,\mathrm{rad/s}$ and $\Gamma_n = 400\,\mathrm{rad/s}$ have been chosen for the numerical simulation and the average is taken over 400 noise realizations for each polar angle θ. The total evolution time is 3 seconds ($\omega_r \approx 2.1\,\mathrm{rad/s}$). The solid line indicates a least-squares fit to the calculated difference $\Delta\phi_g$ using Eq. (18) with the single fit-parameter P as the strength of the noise. The resulting reduced χ^2-value of 1.5 for $P = 138.9\,\mathrm{rad/s}$ indicates the very good agreement between theory and numerical data. The slightly larger noise strength from the fit is due to the non-adiabatic evolution of the state vector leading to a stronger effective perturbation. Note, that we did not take the temporal behaviour of the stochastic process into account, just the static distribution of the random noise. Nevertheless this model turns out to be an excellent approximation.

Numerically, $\Delta\phi_g$ is proportional to $\sin^2\theta_0 \cos\theta_0$ where the proportionality factor depends on the signal-to-noise ratio. This is equivalent to the results found by Whitney and Gefen [15], here based on a more intuitive geometric approach.

6 Proposed experiment

As already noted, due to their spin-1/2 degree of freedom and their weak interaction with the environment neutrons are particularly suitable for experiments on the dephasing behaviour explained above. In particular, ultra-cold neutrons can be stored in appropriate bottles and magnetic fields can be used to manipulate their spin degree of freedom at will. Such a technique is currently used for the precise investigation of a possible electric dipole moment of the neutron [20]. A feasible experimental setup adapted to measurements of Berry's phase in a fluctuating magnetic field is depicted in Figure 4.

Ultra-cold neutrons [21] are produced in a cold source (liquid deuterium at 25 K) and are further decelerated at moving turbine blades resulting in a velocity of about 5 m/s. Those are

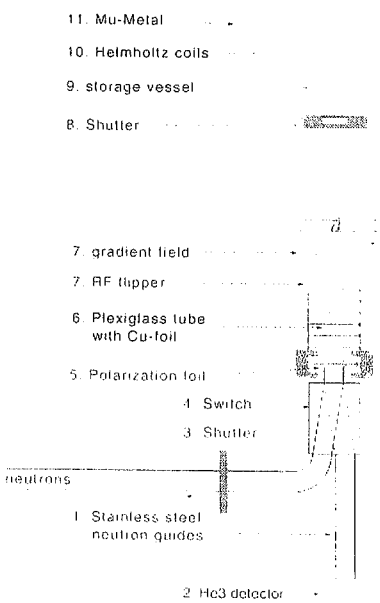

Fig. 4. Schematic setup for storing ultra-cold neutrons and manipulating their spin via Helmholtz-coil pairs.

then guided through evacuated neutron guides to pneumatically controlled shutter and switch. Depending on its position the switch connects the turbine to the storage vessel or the storage vessel to a He-3 detector. A magnetized Fe-foil allowing only for the transmission of neutrons with polarization parallel to its magnetization is used for polarization and – together with a gradient spin-flipper – for analyzation of the spin state. The storage volume itself sits upon a second shutter mechanism and has to be made of non-magnetic material, e.g. polyamide, with an appropriate coating to retain neutrons inside for sufficiently long time without polarization loss. Finally three mutually orthogonal pairs of coils are arranged in an Helmholtz geometry in order to produce a homogeneous field in the center region of the storage box.

After density equilibrium in the apparatus is reached the shutter underneath the storage bottle closes and spin polarized neutrons are retained therein. The critical time scales are then the storage time determined mainly by wall collision losses, the β-decay rate of free neutrons and the longitudinal depolarization time (T1) in the magnetic guide field which is degraded by interactions with stray magnetic fields. A magnetic shielding with a soft magnetic material is advisable to reduce such environmental disturbances. Ramsey interferometry [22] can be utilized to measure the phase difference between positive and negative energy-eigenstate by bracketing the intended cyclic spin evolution in between two $\pi/2$ pulses. The (geometric) phase difference after the evolution can then be measured as a change in the degree of polarization. Since we have full control over magnetic fields it is possible to add artificially fluctuating terms with appropriate strength and frequency spectrum which leads then to a decrease or increase in the visibility of the interference fringes depending on the variance of the phase.

A serious flaw in such experiments is the dephasing time. Inhomogeneous broadening of the resonance width as well as phase differences in the accumulated dynamical phase between different particles due to inhomogeneities in the magnetic field will cause a reduction of the fringe visibility. Numerical studies show that for a homogeneity of the magnetic field less than 0.5% inside the storage volume should allow for decoherence times of the order of one second – sufficient for the intended measurements.

7 Conclusions

Berry's phase and its behaviour in fluctuating fields is an interesting topic both from the conceptual point of view due to its counterintuitive dephasing characteristics – without geometric picture at the back of one's mind its robustness is hardly explicable – and in terms of its utility for high fidelity quantum state manipulation. We have presented numerical data of the variance of the geometric for several noise couplings in view of a prospective experimental realization. Those are in good agreement with a first-order theory, deviations emerge in the non-adiabatic limit for short evolution times, but also for long evolution times due to noise-induced coupling of energy levels. Furthermore, we have shown that the Lamb-shift like offset of the average geometric phase can be explained and calculated quite natural from a mapping of a random variable onto the Bloch-sphere. Eventually, the numerical results demonstrate that the geometric phase is indeed robust against fluctuations in that the variance can be minimized by a proper choice of the evolution time provided that adiabaticity is conserved throughout the operation. Thus, if one succeeds in eliminating the dynamical phase the remaining geometric phase might be a good candidate for error resilient quantum state manipulations.

The author acknowledges support of the Austrian Science Foundation (FWF) Project P18943-N20 and the SFB-F1513 project and wants to thank Y. Hasegawa, J. Klepp, Ch. Plonka and H. Rauch for valuable discussions.

References

1. S. Pancharatnam, Proc. Ind. Acad. Sci. A **44**, 247 (1956)
2. M.V. Berry, Proc. Roy. Soc. Lond. A **392**, 45 (1984)

3. A. Shapere, F. Wilczek (eds.), *Geometric Phases in Physics*, Vol. 5 (World Scientific, Singapore, 1989)
4. Y. Aharonov, J.S. Anandan, Phys. Rev. Lett. **58**, 1593 (1987)
5. J. Samuel, R. Bhandari, Phys. Rev. Lett. **60**, 2339 (1988)
6. F. Wilczek, A. Zee, Phys. Rev. Lett. **52**, 2111 (1984)
7. E. Sjöqvist et al., Phys. Rev. Lett. **85**, 2845 (2000); A. Uhlmann, Rep. Math. Phys. **24**, 229 (1986); S. Filipp, E. Sjöqvist, Phys. Rev. Lett. **90**, 050403 (2003)
8. P. Zanardi, M. Rasetti, Phys. Lett. A **294**, 94 (1999)
9. J.A. Jones, V. Vedral, A. Ekert, G. Castagnoli, Nature **403**, 869 (2000)
10. M.A. Nielsen, I.L. Chuang, *Quantum Computation and Quantum Information* (Cambridge University Press, Cambridge, UK, 2000)
11. S.-L. Zhu, P. Zanardi, Phys. Rev. A **72**, 020301 (2005); I. Fuentes-Guridi, F. Girelli, E. Livine Phys. Rev. Lett. **94**, 020503 (2005)
12. M.S. Sarandy, D.A. Lidar, Phys. Rev. A **73**, 062101 (2006)
13. T. Bitter, D. Dubbers, Phys. Rev. Lett. **59**, 251 (1987); B.E. Allman et al., Phys. Rev. A **56**, 4420 (1997); Y. Hasegawa, G. Badurek, Phys. Rev. A **59**, 4614 (1999); Y. Hasegawa et al., Phys. Rev. Lett. **87**, 070401 (2001); S. Filipp, Y. Hasegawa, R. Loidl, H. Rauch, Phys. Rev. A **72**, 021602 (2005)
14. G. De Chiara, G. Palma, Phys. Rev. Lett. **91**, 090404 (2003)
15. R.S. Whitney, Y. Gefen, Phys. Rev. Lett. **90**, 190402 (2003)
16. N. Wax (ed.) *Selected Papers on Noise and Stochastic Processes* (Dover Publications, New York, 1954)
17. A. Goldberg, H.M. Schey, J.L. Schwartz, Am. J. Phys. **35**, 177 (1967)
18. N.I. Akhiezer, I.M. Glazman, *Theory of Linear Operators in Hilbert space*, Vol. 2 (Dover Publications, Inc., New York, 1993)
19. S.O. Rice, Bell Syst. Techn. J. **23**, 282 (1944); Bell Syst. Techn. J. **24**, 46 (1944), also published in [16]
20. C.A. Baker et al., Phys. Rev. Lett. **97**, 131801 (2006)
21. R. Golub, D.J. Richardson, S.K. Lamoreaux, *Ultra-Cold Neutrons* (Adam Hilger, Bristol, 1991)
22. N.F. Ramsey, *Molecular Beams* (Oxford Univ. Press, New York, London, 1956)